



A high-resolution pollen record from East China reveals large climate variability near the Northgrippian-Meghalayan boundary (around 4200 years ago) exerted societal influence

Chun-Hai Li^{a,*}, Yong-Xiang Li^{b,*}, Yun-Fei Zheng^c, Shi-Yong Yu^d, Ling-Yu Tang^e, Bei-Bei Li^f, Qiao-Yu Cui^g

^a State Key Laboratory of Lake Science and Environments, Nanjing Institute of Geography and Limnology, Chinese Academy of Sciences, Nanjing 21008, China

^b Key Laboratory of Surficial Geochemistry, Ministry of Education, State Key Laboratory for Mineral Deposits Research, School of Earth Sciences and Engineering, Nanjing University, Nanjing 210046, China

^c Zhejiang Provincial Institute of Cultural Relics and Archaeology, Hangzhou 310014, China

^d School of Geography, Geomatics, and Planning, Jiangsu Normal University, Xuzhou 221116, China

^e Nanjing Institute of Geology and Palaeontology, Chinese Academy of Sciences, Nanjing 210008, China

^f Institute for History of Science and Technology, Nanjing University of Information Science and Technology, Nanjing 210044, China

^g Institute of Geographical Sciences and Natural Resources Research, Chinese Academy of Sciences, Beijing 100101, China

ARTICLE INFO

Keywords:

ENSO
Asian summer monsoon
Vegetation history
Climate change
Neolithic culture
Zhejiang Province, Northgrippian-Meghalayan boundary

ABSTRACT

The large and rapid climate change event that occurred around 4200 years ago (hereafter the 4.2-kyr event that marks the onset of the Meghalayan stage) is one of the most significant climatic anomalies in the Holocene. It may have exerted profound societal impact globally; however, its triggering mechanism remains uncertain. Here we present a high-resolution, well-dated pollen record covering this interval from the Tianluoshan archaeological site in East China. Our results show that the hydroclimatic conditions in the study area across this event strikingly resembled the regional expression of modern El Niño-Southern Oscillation (ENSO) and exhibited interdecadal ENSO-like variability from ca. 4.50 to 4.00 cal kyr BP. Also, our pollen data indicate a marked shift toward an overall increased intensity and frequency of ENSO-like climate variability from ca. 4.50 to 4.30 cal kyr BP, which was immediately followed by a decline of rice-based agriculture, providing direct evidence for the causal link between climate deterioration and the collapse of Neolithic civilization in East China some 4200 years ago. This observation is in accord with the enhanced ENSO variability reconstructed from proxy records in the tropical Pacific Ocean. As ENSO is intimately coupled with the Asian summer monsoon and the Intertropical Convergence Zone (ITCZ), we suggest that the enhanced ENSO-like climate variability may have triggered the 4.2-kyr event.

1. Introduction

The large and rapid climatic changes occurring in the wake of the Last Deglaciation are generally ascribed to freshwater disturbance on the North Atlantic thermohaline circulation (e.g., Broecker et al., 1989; Meissner and Clark, 2006; Yu et al., 2010; Li et al., 2012a). As major continental ice sheets had melted completely by about 7 kyr BP (Lambeck et al., 2014), the Earth's climatic system reorganized and evolved into a configuration similar to that of today. The 4.2-kyr event, ranging from 4.40–4.00 cal kyr BP, marks the Northgrippian-Meghalayan boundary and represents a major climatic anomaly in the second half of the Holocene, and it is manifested as intensified cooling in high

latitudes and enhanced aridification in middle and low latitudes (Bond et al., 2001; Mayewski et al., 2004; Booth et al., 2005; Walker et al., 2012). This event is believed to have exerted profound impacts on Neolithic civilizations in many areas of the world (Weiss and Bradley, 2001; Staubwasser et al., 2003; Liu and Feng, 2012; Dixit and Hodell, 2014; Prasad et al., 2014; Ruan et al., 2016) and is thus of great societal relevance, particularly within the context of present-day global warming. However, the triggering mechanism of this event remains uncertain (Meehl, 1994; Bond et al., 2001; Haug et al., 2001; Barron and Anderson, 2011).

A growing body of evidence shows that climate deteriorated in many areas of China during the Neolithic-Bronze Age transition

* Corresponding authors.

E-mail addresses: chhli@niglas.ac.cn (C.-H. Li), yxli@nju.edu.cn (Y.-X. Li).

<https://doi.org/10.1016/j.palaeo.2018.07.031>

Received 10 March 2018; Received in revised form 27 July 2018; Accepted 27 July 2018

Available online 03 August 2018

0031-0182/ © 2018 Elsevier B.V. All rights reserved.

corresponding to the 4.2-kyr event, which may have exerted a devastating impact on Chinese civilization (Wu and Liu, 2004). For example, the intensified drought or flooding may have been thought as the culprit of the demise of the Neolithic culture in China (Wu and Liu, 2004; Liu and Feng, 2012). The Yangtze River Delta has a long history of human occupation from the Neolithic period onward. Archaeological excavations in this area revealed several cultural disruptions (Zhu et al., 1996; Yu et al., 2000; Zhang et al., 2004). The fall of the Neolithic civilization in the wake of the Liangzhu cultural period (4.50–4.00 kyr BP) represents a major societal transition, which has been ascribed to the large and rapid climate and environmental changes corresponding to the 4.2-kyr event (Atahan et al., 2008; Zong et al., 2012; Innes et al., 2009). However, the nature of this link is still a matter of long-standing debate (Zong et al., 2012).

The major hindrance to testing the proposed human-climate link in this area is the absence of reliable chronological constraints on the cultural and climate changes during the second half of the Holocene, especially the critical period of 4.50–4.00 cal kyr BP (Wang, 2017; Li et al., 2014). Therefore, more work is needed to establish a robust chronological framework for the proxy records of Holocene climate and environmental changes in this area. Here, we present a high-resolution, well-dated pollen record that may help elucidate the dynamics of climate changes and their potential societal impact in this area across the 4.2-kyr event. The pollen record has been shown in Li et al. (2012b). In this study, we present six newly obtained ^{14}C ages that cover the upper part of the pollen record and re-interpret the results.

2. Study area

The Ningshao Plain is a low-lying coastal mudflat situated in the Lower Yangtze Valley (LYV) in East China (Fig. 1A, B). Influenced by the East Asian Monsoon, climate in this area exhibits a remarkable seasonality with coherent changes in temperature and precipitation. According to the instrumental record (1951 CE–2005) at the Cixi Meteorological Station, modern mean annual temperature is 16.2 °C with mean January temperature of 4.2 °C and mean July temperature of 28.2 °C. Annual precipitation is around 1600 mm, most of which occurs in the summer. This area is sensitive to tropical climate variations such as ENSO, which modulates the East Asian Monsoon system via complex ocean-atmospheric interactions (Wang et al., 2000; Kim et al., 2014). Instrumental records and modeling show that climate of the LYV area is characterized by a weakened East Asian Monsoon during El Niño years, usually leading to warm winters, cool summers, and increased precipitation (Li, 1989; Zhao, 1989; Chen, 1995; Yuan et al., 2012; Kim et al., 2014). Conversely, climate during La Niña years is characterized by a strengthened East Asian Monsoon, resulting in cold winters and decreased precipitation (or dry conditions) in the summer.

Vegetation in East China is composed mainly of subtropical mixed forests of evergreen and deciduous trees. Oaks including *Quercus* and *Cyclobalanopsis* (sometimes considered a subgenus of *Quercus*) are the dominant elements in the studied area; these include two ecological types, deciduous oak species comprising *Quercus aliena*, *Q. acutissima*, *Q. variabilis*, *Q. fabri*, among others and evergreen oak species, including *Cyclobalanopsis myrsinaefolia*, *C. myrsinifolia*, *C. gambleana* and *C. multinervis* (Wu, 1980). Evergreen trees are dominated by *Lithocarpus*, *Cyclobalanopsis*, and *Quercus*, while the deciduous trees mainly

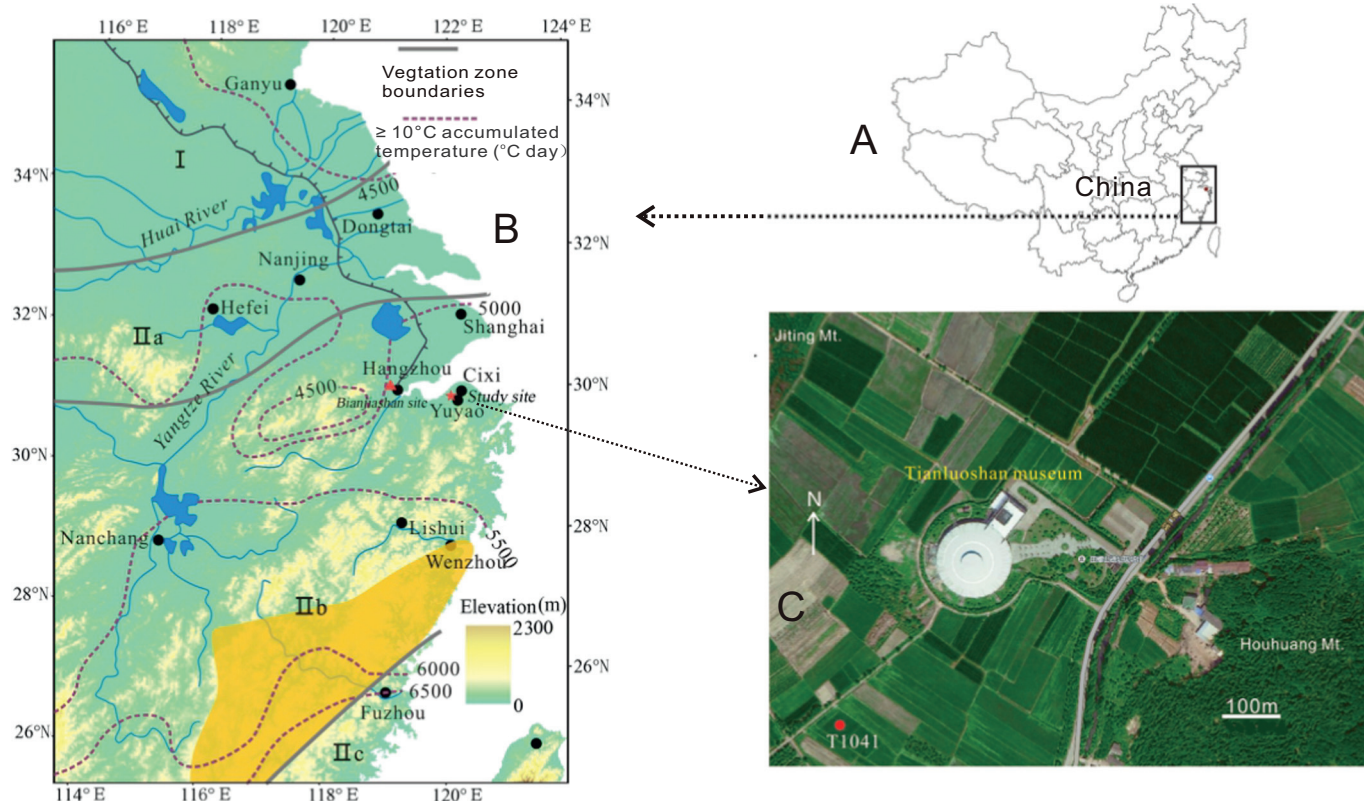


Fig. 1. Maps showing the location of the Tianyunshan archaeological site and the biogeography of East China. (A) The location of the study area in China. (B) Biogeography of temperature-sensitive tree species in East China. Brown shaded area indicates the occurrence of *Altingia* and vegetation zones are also marked as follows: temperate deciduous broad-leaved forest (I) and the mixed forest of subtropical evergreen and deciduous broad-leaved forest (IIa-northern, IIb-central, and IIc-southern subzone). The red star indicates the location of Tianyunshan area shown in (C) and the red triangle mark the Bianjiashan archaeological site where *Altingia* fossil wood and wood utensils were excavated. (C) Red dot indicates the location of the studied trench T1041. (For interpretation of the references to color in this figure legend, the reader is referred to the web version of this article.)

consist of *Liquidambar*, *Castanea*, *Aphananthe*, *Celtis*, and *Ulmus*.

The topography of East China is characterized by low lying plains and the vegetation in East China exhibits distinct latitudinal zonation following a temperature gradient (Fig. 1B). Huaihe River roughly marks the boundary (~33°N to 34°N) between the warm temperate deciduous broad-leaved forest (i.e., Zone I) to the north and the subtropical forest (i.e., Zone II) to the south (Fig. 1B). Within the subtropical forest, the composition of tree species is governed by the temperature of the coldest month (> 0 °C) and the accumulated temperature for the ≥10 °C temperature (Wu, 1980), which is mainly controlled by the summer temperatures in East China. Therefore, the subtropical forest is further subdivided into three subzones, i.e., the northern (i.e., Zone IIa), the central (i.e., Zone IIb), and the southern (i.e., Zone IIc) zones. IIa, IIb, and IIc represent the northern subtropical mixed evergreen forest and deciduous broad-leaved forest, the middle subtropical evergreen broad-leaved forest, and the southern subtropical evergreen broad-leaved forest, respectively.

The Tianluoshan archaeological site studied here was mainly occupied during the Hemudu period (7000–5500 cal yr BP). The site is located in the central north of Zone IIb (Fig. 1B). The natural vegetation is subtropical evergreen broadleaved trees, which can be found occasionally in mountainous areas nowadays due to long-term agricultural activities. Most of the primitive areas have been disturbed and turned to croplands and secondary forests.

3. Methods

3.1. Radiocarbon dating

Additional samples were collected from Trench 1041 (30°01.355'N, 121°22.648'E) at the Tianluoshan site (Fig. 1C) to obtain a firm chronological framework. A previous study has established the general framework of the chronostratigraphy of the Trench (Li et al., 2012b). This high-resolution study focuses on the interval across the 4.2-kyr event. Six AMS ¹⁴C ages were obtained from terrestrial plant remains and *Bulrush* seeds extracted from three consecutive stratigraphic sections (i.e., 80–75 cm, 75–70 cm, and 70–65 cm) (Table 1). The AMS ¹⁴C dates were calibrated using the OxCal 4.3.2 computer program (Bronk Ramsey, 2009) in conjunction with the IntCal13 tree-ring calibration dataset (Reimer et al., 2013). The age-depth model was constructed with Bacon, a flexible Bayesian age-depth modeling tool that takes into account of different sources of uncertainty (Blaauw and Christen,

2011). This approach involves dividing the Tianluoshan profile into 38 sections at 5 cm intervals and performing millions of Markov Chain Monte Carlo (MCMC) iterations to obtain an optimal age-depth model.

3.2. Pollen analyses

Standard HF method was used for the pretreatment of the samples (Faegri et al., 1989), and the exotic *Lycopodium* spores (22,340 spores per tablet) were added as markers to allow the calculation of pollen concentrations. A minimum of 500 pollen grains was counted for each sample (the minimum is 527 grains and average is 967 grains).

Oaks are the dominant species in the study area and they can be divided into two types, evergreen oaks (including evergreen *Quercus* and *Cyclobalanopsis*) and deciduous oaks (deciduous *Quercus*). It is crucial to accurately identify these two different ecological categories of oak pollen. Liu et al. (2007) examined the living and fossil pollen of these two types of oaks and showed that it is difficult to distinguish evergreen *Quercus* and deciduous *Quercus* pollen globally because a similar shape and ornamentation can occur in both types across different regions, notably North American and Asia, or in some areas such as mountainous regions of SW China. But in other regions, dominant exine sculptures can be used to differentiate evergreen and deciduous pollen types, such as in Zhejiang, East China where Liu et al. (2007) showed that Miocene evergreen and deciduous oaks pollen can be discriminated based on pollen size, shape, and ornamentation.

Our study site is also situated in Zhejiang, East China. It is expected that Holocene evergreen and deciduous oak pollen from the study area can be discriminated as well. As such, the pollen of *Cyclobalanopsis* is distinguished from that of deciduous *Quercus* based on previous works (Wang et al., 1997; Wang and Chang, 1991; Liu et al., 2007) and our collections of modern pollen samples. The following criteria are used to distinguish the pollen of the evergreen and deciduous oaks. In general, evergreen *Quercus* pollen is prolate, diameter is < 30 μm, 3-colporate or 3-colporoidate, its exine sculpture is smooth or finely granulate. In contrast, deciduous *Quercus* pollen is subspheroidal, diameter is > 30 μm, most grains are 3-porate, few grains are 3-colporoidate, and its exine sculpture is obviously tuberculate.

Table 1
AMS ¹⁴C dates from Trench 1041, Tianluoshan, Zhejiang Province, China.

Depth	Materials	AMS	Radiocarbon age		Calibrated age (cal yr BP)			Source
(cm)	Dated	Lab #	(¹⁴ C yr BP)	± 1σ	Mid-point	± 2σ	2σ range	
65–70	Plant remains	Poz70204	3840	50	4255	160	4415–4095	This study
70–75	Plant remains	BA398102	3970	30	4410	110	4525–4300	This study
70–75	Seeds	Poz66934	3810	70	4200	215	4415–3990	This study
75–80	Plant remains	Poz69037	4000	70	4525	280	4810–4245	This study
75–80	Seeds	Poz69036	3890	35	4300	115	4420–4185	This study
75–80	Seeds	BA398100	3830	30	4250	150	4405–4100	This study
81–86	Plant remains	BA07762	3760	40	4115	130	4245–3985 ^a	Li et al., 2012b
96–101	<i>Yagara bulrush</i>	BA07761	4015	45	4575	215	4790–4360 ^a	Li et al., 2012b
106–111	<i>Bulrush</i>	BA07760	4195	70	4705	160	4865–4545 ^a	Li et al., 2012b
121–126	<i>Bulrush</i>	BA08203	4470	45	5130	170	5305–4960 ^a	Li et al., 2012b
131–136	<i>Yagara bulrush</i>	BA07758	4765	35	5460	130	5590–5330 ^a	Li et al., 2012b
136–141	<i>Yagara bulrush</i>	BA08895	4830	35	5560	85	5645–5475 ^a	Li et al., 2012b
141–146	<i>Yagara bulrush</i>	BA08894	4965	35	5730	125	5855–5605 ^a	Li et al., 2012b
146–151	<i>Yagara bulrush</i>	BA08893	5040	40	5785	115	5905–5665 ^a	Li et al., 2012b
223–228	<i>Flatstalk bulrush</i>	BA07764	5785	60	6590	140	6730–6450 ^a	Li et al., 2012b
228–233	<i>Flatstalk bulrush</i>	BA07763	6045	45	6945	190	7140–6755 ^a	Li et al., 2012b

Note: AMS = accelerator mass spectrometry. BA = Beta AMS lab. Poz = Poland AMS lab. Calibration is based on OxCal 4.3.2.

(Bronk Ramsey, 2009) using IntCal 13 atmospheric curve (Reimer et al., 2013).

^a Recalibrated from the original source. All ages are rounded to the nearest 5 years.

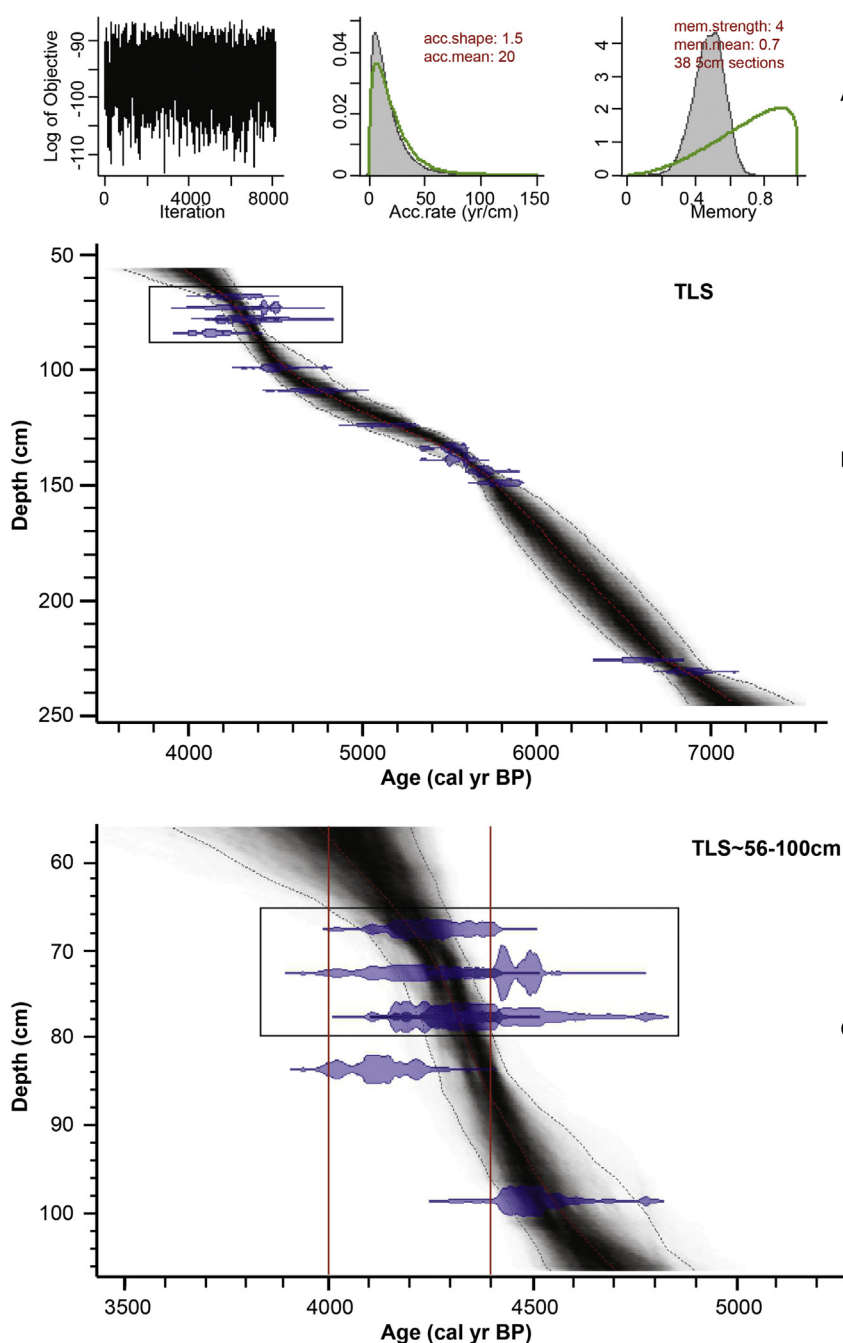


Fig. 2. Age-depth model of trench T1041 established using Bacon, a flexible Bayesian age-depth modeling tool that takes into account of different sources of uncertainty (Blaauw and Christen, 2011). (A) Major parameters used to assess the quality of the age-depth model; stored MCMC (Markov Chain Monte Carlo) iterations (left panel; good runs show a stationary distribution with little structure among neighboring iterations); the prior (green curves) and posterior (grey histograms) distributions for the accumulation rate (middle pane) and its memory (right panel; defines how much the accumulation rate of a particular depth in a core depends on the depth above it). Abbreviations: acc. = accumulation; mem. = memory. (B) The established age-depth model for trench T1041 profile based on the six AMS ^{14}C dates obtained in this study (marked with a rectangular) and the AMS ^{14}C dates from Li et al. (2012b). (C) The close-up of the upper part of the stratigraphy in this study focusing on the 4.2-kyr event constrained by the additional six AMS ^{14}C dates. The two red lines demarcate the age interval of ~4.40–4.00 cal kyr BP that was defined based on the depth interval of 80–65 cm for the six AMS ^{14}C dates of this study. These dates provide tight chronological constraints on the 4.2-kyr event at the Tianluoshan site. (For interpretation of the references to color in this figure legend, the reader is referred to the web version of this article.)

4. Results

4.1. Age-depth model

All ^{14}C ages from the Tianluoshan site are presented in Table 1 and the chronology in Fig. 2. The stationary distribution of the MCMC (Markov Chain Monte Carlo) iterations (Fig. 2A) indicates that the age-depth model for the Tianluoshan site (Fig. 2B) is a good run and the accumulation rate at Tianluoshan during 7000–4000 cal yr BP is relatively stable. The calibrated ages of the six new ^{14}C ages of samples retrieved from 65 cm to 80 cm range from 4400 to 4000 cal yr BP. (Fig. 2C), and these new ages provide a tighter chronological constraint on the 4.2-ka event (Fig. 2).

4.2. Pollen data

The pollen data show two major intervals of large variations in pollen abundance, i.e., one from ~6.10 to 5.90 cal kyr BP and the other from ~4.50 to 4.00 cal kyr BP (Fig. 3). The ~6.10 to 5.90 cal kyr BP interval is characterized by a dramatic increase in the abundance of deciduous *Quercus* species (Fig. 3A), deciduous oaks mainly grow in temperature area or high elevation mountains in the subtropical area in East China (Wu, 1980). So, the increase of deciduous *Quercus* indicates cool summers. This increase is accompanied by the absence (or extremely low abundance) of *Altingia* (Fig. 3A), suggesting a major cooling in both winters and summers around 6.00 cal kyr BP. This major cooling event may represent the response to a weakened East Asian Monsoon (Wang et al., 2005; Liu et al., 2014) that is probably related to the ~6.00 cal kyr BP cold event in the North Atlantic realm (Bond et al., 2001).

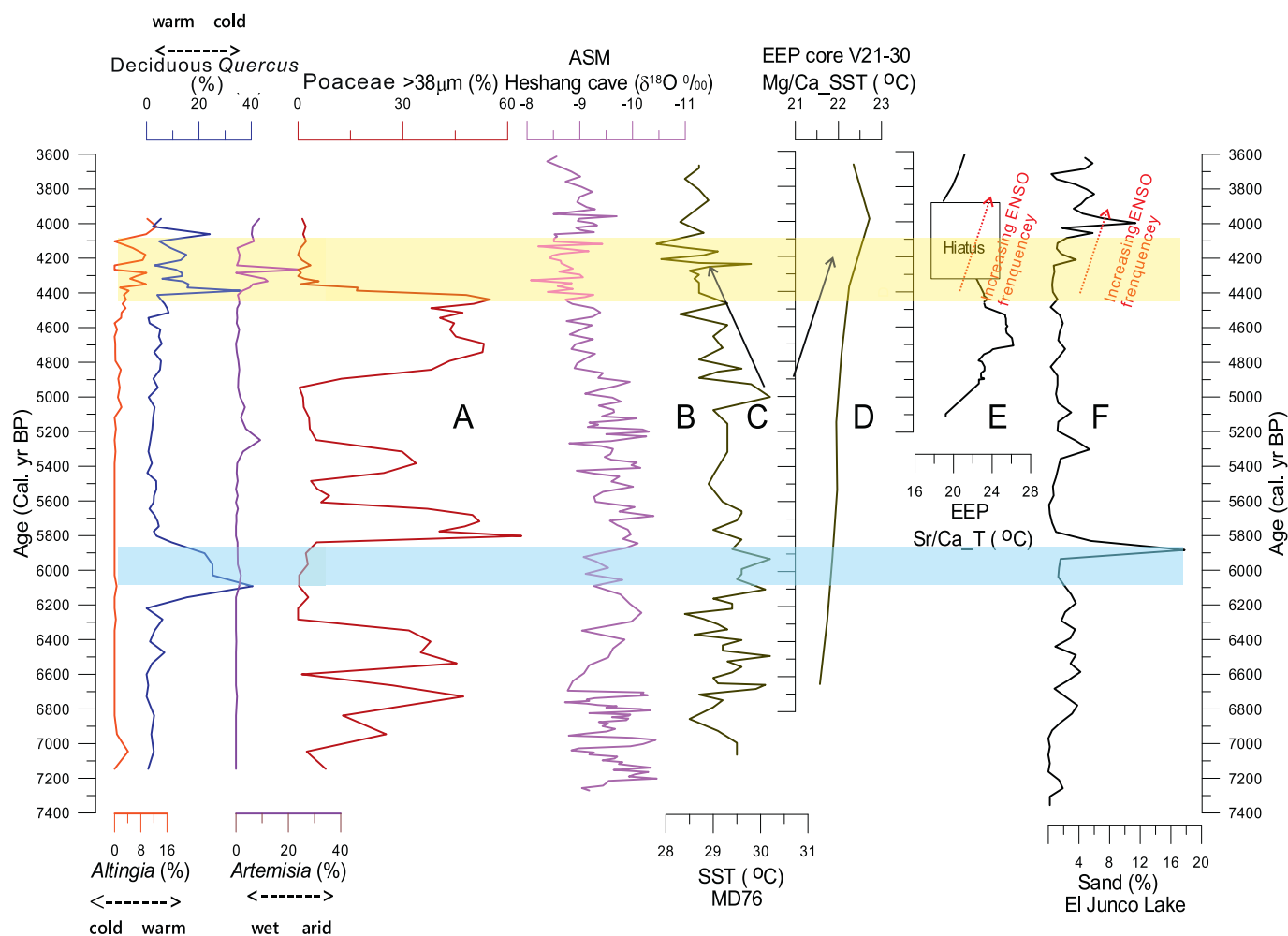


Fig. 3. Comparison of pollen data from trench T1041 of the Tianluoshan site (A) with the proxy record of Asia Monsoon (B) and the sea surface temperature (SST) and precipitation proxy records from tropical Pacific (C–F). (A) Pollen data from trench T1041 at Tianluoshan archaeological site; (B) Speleothem $\delta^{18}\text{O}$ record from Heshang Cave, South China (Hu et al., 2008); (C) and (D, E) are proxy records of SST from the equatorial west Pacific (Stott et al., 2004) and east Pacific (Koutavas et al., 2002; Toth et al., 2015), respectively; (F) Grain size of sands from El Junco Lake, Galápagos, a proxy for ENSO-related precipitation in equatorial east Pacific (Conroy et al., 2008).

The ~4.50 to 4.00 cal kyr BP interval is characterized by large variations in the abundance of *Altingia*, deciduous *Quercus*, *Artemisia*, and *Poaceae* (Fig. 3A). The abundance of both *Altingia* and deciduous *Quercus* fluctuates, which is accompanied by an overall rapid increase and a subsequent decrease in *Artemisia* as well as an overall dramatic decrease in the abundance of large *Poaceae* (> 38 μm) between ~4.50 and 4.00 cal kyr BP (Fig. 3A). The large *Poaceae* (> 38 μm) is used as a rice indicator (Li et al., 2012b). Within this time interval, the generally high abundance of deciduous *Quercus* indicates overall cool summers. The relative increase in the abundance of deciduous *Quercus* may indicate cooler summers (Fig. 4). *Altingia* exhibits presence, indicating warm winters (Fig. 4). Similarly, the relative increase or decrease in the abundance of *Altingia* may also indicate subordinate warmer or cooler winters.

One striking feature of the ~4.50 to 4.00 cal kyr BP interval is that the occurrence of *Altingia* appears to correspond to intervals of the absence or very low abundance of *Artemisia* (Fig. 4, blue bands) and the absence of *Altingia* corresponds to intervals of increased abundance of *Artemisia* (Fig. 4, yellow bands). One notable exception occurs at the interval from ~4.34 to 4.26 cal kyr BP when both *Altingia* and *Artemisia* show high abundance (Fig. 4, pink band). Interestingly, within this interval, the decrease in the abundance of *Altingia* appears to correspond to the increase in the abundance of *Artemisia*, and vice versa (Fig. 4, arrows). It appears that the fundamental relationship of high/

low abundance of *Altingia* corresponding to low/high abundance of *Artemisia* persisted from ~4.50 to 4.00 cal kyr BP. *Artemisia* is a proxy for precipitation with high/low abundance indicating dry/wet periods (Zheng et al., 2008). Therefore, intervals of the high abundance of *Altingia* and low abundance of *Artemisia* indicate periods of warm winters and wet climate (Fig. 4, blue bands). These intervals are also marked by an overall relative increase in the abundance of deciduous *Quercus*, indicating subordinate cooler summers. Conversely, intervals of the absence of *Altingia*, the high abundance of *Artemisia*, and the subordinate decrease in the abundance of deciduous *Quercus* (Fig. 4, yellow bands) indicate periods of cold winter, relatively warm summer, and dry conditions. Large *Poaceae* (> 38 μm) is a proxy for farming of cultivated rice by early humans in East China (Li et al., 2012b). In the ~4.50 to 4.00 cal kyr BP interval, the abundance of large *Poaceae* (> 38 μm) displays an abrupt decline at around 4.32 cal kyr BP and remained at very low abundance or absence afterwards (Fig. 4), rice spikelets and rice phytoliths also nearly disappear (Li et al., 2012b), suggesting a rapid collapse of the rice-based society at ~4.32 cal kyr BP.

5. Discussion

5.1. Pollen resource and proxies

The Tianluoshan site is located in a generally low-lying area and

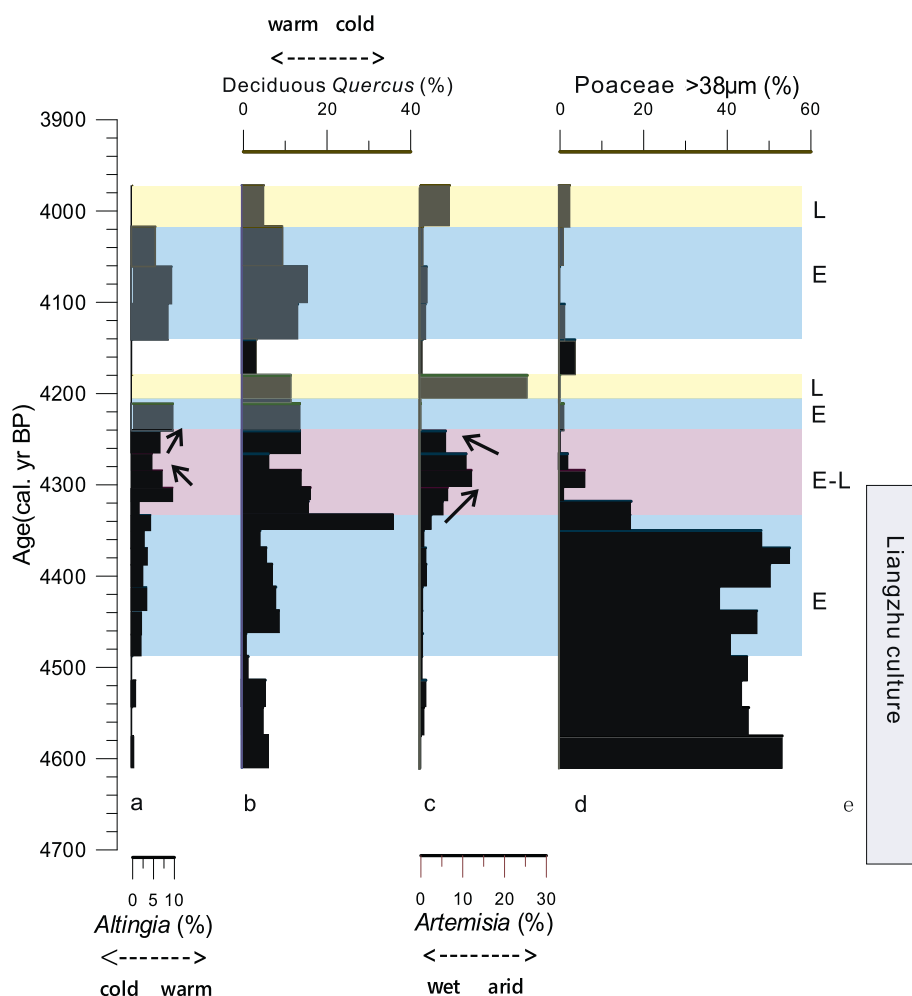


Fig. 4. Variations in the abundance of temperature- and precipitation-sensitive pollen types from ~4.50 to 4.00 cal kyr BP reveal prolonged periods of El Niño dominated ('E', blue bands), La Niña dominated ('L', yellow bands), and ENSO dominated ('E-L', pink band) climate variability in the study area. *Altingia*, a proxy for winter temperature; deciduous *Quercus*, a proxy for summer temperature; *Artemisia*, a proxy for precipitation; Poaceae > 38 μm, a proxy for farming of cultivated rice in East China. Pollen samples were collected consecutively and each horizontal bar represents one pollen sample. Note changes in the thickness of the horizontal bars, indicating varying temporal resolutions of the pollen records. The rectangle indicates the late period of the Liangzhu culture (after Wang et al., 2017). (For interpretation of the references to color in this figure legend, the reader is referred to the web version of this article.)

wetlands were present in the relatively flat regions (Zhang et al., 2004; Li et al., 2012b). Plant macrofossils and phytolith assemblages show that the local vegetation was dominated by phragmite, rice, sedge, and several other upland herbs, and no woody plant macrofossils were found. Therefore, arboreal and most of the upland herbaceous pollen grains found at this site were derived from the neighboring high mountains, while most of the Poaceae, Cyperaceae, and aquatic pollen grains found at this site were derived from the proximal wetlands.

5.1.1. Poaceae > 38 μm

Rice pollen grains in sediments and topsoil demonstrate that Poaceae with a size > 35 μm might represent the existence of rice agriculture. Palynological work on modern topsoil shows that the percentage of Poaceae > 35 μm pollen usually exceeds 40% in modern paddy fields (Yang et al., 2012). Previous studies in the Yangtze Delta also show the dominance of Poaceae > 35 μm pollen in ancient paddy fields. A larger diameter was generally used to differentiate the domesticated rice from the wild Poaceae (Itzstein-Davey et al., 2007; Innes et al., 2009; Shu et al., 2010; Li et al., 2012b; Long et al., 2014; Liu et al., 2016). All Poaceae grains are > 38 μm in the studied profiles; therefore, we use Poaceae > 38 μm as an indication for the presence of domesticated rice in the study area.

Altingia is an evergreen broad-leaved tree belonging to the family of Hamamelidaceae. At present, there are two main types of *Altingia* (i.e., *Altingia chinensis* and *Altingia gacilipes*) in the Zhejiang area. *Altingia* grows relatively fast. It typically takes 8 to 9 years to flower and 20 years to fructify (Long et al., 2009). The seeds of *Altingia* are small, which is conducive for propagation. Modern *Altingia* occurs in the

southern part of the mid-subtropical vegetation zone and south-subtropical vegetation zone and its northernmost limit of occurrence is near Wenzhou city at ~28°N (Fig. 1B, brown shaded area). Data from the East Asian modern topsoil pollen database show that *Altingia* pollen occurs only in South China (Zheng et al., 2014, Appendix S3). *Altingia* owes its existence to the fact that winter temperatures in areas south of Wenzhou city are higher than other parts of Zhejiang, because the northeast-striking mountain belt blocks cold air mass to penetrate to the south in winter. The mean temperature of the coldest month (January) of a year is the limiting factor for *Altingia*'s growth. It can only survive when the mean temperature of the coldest month (January) is > 5 °C (Chen et al., 1988).

Deciduous *Quercus* is an important element in subtropical mixed evergreen and deciduous forest and it is also a dominant species in temperate deciduous broad-leaved forests, which includes *Q. aliena*, *Q. acutissima*, *Q. variabilis*, *Q. fabri*, and so on (Wu, 1980). Abundant deciduous *Quercus* only occurs in areas north of Shanghai (~31°N) (Fig. 1B). The present-day boundary between temperate and subtropical forests is located along the Qingling-Huaihe River (~33° to 34°N) (Fig. 1B). Between the Qingling-Huaihe River and Shanghai, deciduous *Quercus* competes with subtropical species including the *Quercus* evergreen-type (hereafter collectively referred to as *Quercus* E), including *Castanopsis* and *Cyclobalanopsis* etc. that are also controlled by the ≥ 10 °C accumulated temperature. The relative abundance of deciduous *Quercus* and subtropical species are governed by January temperatures and ≥ 10 °C accumulated temperature (mainly reflecting summer temperature). The abundance of deciduous *Quercus* decreases and that of subtropical species increases with decreasing latitudes.

Accordingly, an increase in January temperatures and the $\geq 10^\circ\text{C}$ accumulated temperature may lead to a decrease in the relative abundance of deciduous *Quercus* and an increase in the relative abundance of subtropical species, and vice versa. Therefore, an increase in the relative abundance of deciduous *Quercus* occurs when cool summers prevail (Wu, 1980). Deciduous *Quercus* prefers sunny environment and thus its occurrence may indicate relatively arid conditions. However, in areas of humid maritime climate in the eastern China, temperature is a limiting factor for deciduous *Quercus* (Wu, 1980), whereas in arid North China, deciduous *Quercus* indicates warm and humid climate (Yi et al., 2013).

Artemisia is a dominant species of grasslands in China, but its pollen mainly occurs ($> 30\%$) in arid steppe where annual precipitation is relatively low (Zheng et al., 2008). According to the pollen-climate relationship based on 461 topsoil samples in North China, herbaceous plants (mainly Chenopodiaceae and *Artemisia*) indicate arid climate, while the abundance of arboreal plants is positively correlated with humidity (Yi et al., 2013). However, *Artemisia* pollen may have relatively high abundance in areas of high precipitation (Zheng et al., 2008), usually indicating intensive human agricultural activities (Li et al., 2015). Therefore, high abundance of *Artemisia* pollen may indicate reduced precipitation and dry climate in East China if the influence of human activities can be ruled out.

5.2. The ~ 7.0 to 4.0 cal kyr BP vegetation history

The vegetation of the study area was dominated by subtropical evergreen forest and experienced six phases of evolution from ~ 7.00 to 4.20 cal kyr BP (Li et al., 2012b). There were two prominent phases, one from ~ 6.10 to 5.80 cal kyr BP and the other from ~ 4.60 to 4.00 cal kyr BP, when the abundance of deciduous *Quercus* increased and the subtropical evergreen forests gave rise to the mixed evergreen and deciduous broad-leaved forests.

5.3. Mid-Holocene climate changes during 4.50–4.00 cal kyr BP

The substantial increases in the abundance of deciduous *Quercus* pollen at 6.10–5.80 cal kyr BP and 4.60–4.10 cal kyr BP indicate two cold events occurring during the middle Holocene. These events recognized at the Tianluoshan site (Fig. 3A) are also documented in other records in the Lower Yangtze Valley (Innes et al., 2009). Analyzing the temperature-sensitive tree species at the Tianluoshan site reveals a distinct nature of these two cooling intervals. For example, *Altingia* was in low abundance or absent during ~ 6.10 –5.80 kyr BP, indicating cool summers; whereas the abundance of *Altingia* fluctuated between 4.50 and 4.00 kyr BP, suggesting temperature variations in both winters and summers. Plant macrofossils, phytolith, and pollen data from this area suggest that there were no agricultural activities during these two cooling intervals (Zheng et al., 2008; Li et al., 2012b). In fact, recent studies show that human activities in the lower Yangtze Valley dramatically weakened after ~ 4.60 kyr BP (Innes et al., 2009; Wang et al., 2017). Therefore, changes in pollen assemblage within these two intervals, including variations in the abundance of *Artemisia*, should indicate vegetation responses to climate change rather than human activities.

High-resolution pollen data show that variations in the pollen abundance between ~ 4.50 kyr BP and 4.00 kyr BP constitute three types of time intervals denoted by blue, yellow, and pink bands (Fig. 4). The first type, or the ‘E’ type as indicated in blue bands (Fig. 4), is characterized by the occurrence of abundant *Altingia*, relatively increase in deciduous *Quercus*, and the very low abundance of *Artemisia*, indicating periods of warm winters, (subordinate) cool summers, and wet conditions. The second type, or the ‘L’ type as indicated in yellow bands (Fig. 4), is featured by the absence of *Altingia*, relatively subordinate decrease in deciduous *Quercus*, and the increased abundance of *Artemisia*, indicating periods of cold winters, warm summers, and dry

conditions. The third type, or the ‘E–L’ type as indicated in a pink band (E–L, Fig. 4), characterizes the time interval at around 4.3 kyr BP, which shows generally high abundance of *Altingia*, deciduous *Quercus*, and *Artemisia*. The decrease (increase) in the abundance of *Altingia* corresponds to the increase (decrease) in the abundance of *Artemisia*.

The physiological properties of *Altingia* can provide additional insight into the duration of the warm winter and cool summer conditions. *Altingia* needs at least 8–9 years to begin to flower and about 20 years to fructify. Also, abundant fossil *Altingia* woods are found at the Liangzhu culture site (Zhejiang Provincial Institute of Cultural Relics and Archaeology, 2014), corroborating that *Altingia* trees grew extensively in this region during 4.50–4.20 cal kyr BP. Therefore, the occurrence of macrofossil *Altingia* in the study area implies that warm winter conditions persisted for at least 8–9 years and probably longer, thus indicating an anomalously prolonged (> 8 years, maybe decadal), the occurrence of *Altingia* appears continuously in the strata. For instance, the six consecutive 2-cm thick samples between 4.46 and 4.34 cal kyr BP and the three consecutive samples between 4.14 and 4.02 cal kyr BP (Fig. 4) yield abundant *Altingia* pollen, suggesting a ~ 120 -year period of warm winter. For the ‘E–L’ interval, i.e., 4.34 to 4.24 cal kyr BP, we are unable to differentiate these two climate states due to the low temporal resolution of the samples, but the E and L type may occur alternatively, lasting for about 100 years. Overall, the E and L types characterized the climate changes during 4.50–4.00 cal kyr BP.

5.4. A regional expression of the ENSO-like climate pattern during 4.50–4.00 cal kyr BP

Instrumental records and climate modeling results show that modern ENSO could exert significant impacts on the terrestrial climate in East China via affecting the strength of East Asian Monsoon (EAM) (Wang et al., 2000). Modern ENSO is an interannual variation in sea-surface temperatures (SST) and atmospheric pressure over tropical Pacific (McPhaden et al., 2006). Warming (cooling) in equatorial East Pacific (EEP) and cooling (warming) in equatorial West Pacific (EWP) leads to El Niño (La Niña) years (McPhaden et al., 2006). During El Niño years, cooling in EWP would weaken EAM and result in warm winter, cool summer, and wet climate in East China (Li, 1989; Zhao, 1989; Chen, 1995; Gong and Wang, 1999; Yuan et al., 2012; Kim et al., 2014). The climatic conditions of modern La Niña state led to the East Asian Monsoon strengthens and precipitation decrease in the LYV (Wang et al., 2000; Yuan et al., 2012; Kim et al., 2014). Pollen data from the Tianluoshan site show a climate pattern consistent with the dominance of ENSO climate variability from ~ 4.50 to 4.00 cal kyr BP (Fig. 4), and $\delta^{18}\text{O}$ data of speleothem from South China document a weakened East Asian Summer Monsoon during this interval (Hu et al., 2008) (Fig. 3b), which is compatible with the prevailing ENSO conditions in tropical Pacific (Wang et al., 2000; Sun, 2000) and is particularly due to cooling in West Pacific (Stott et al., 2004). Indeed, proxy records show that equatorial West Pacific (EWP) underwent a cooling (Stott et al., 2004) and equatorial East Pacific (EEP) experienced a warming from ~ 4.50 to ~ 4.00 cal kyr BP (Koutavas et al., 2002) (Fig. 3C–F). The work of Koutavas et al. (2002) also revealed a warming in the equatorial East Pacific and a cooling in the equatorial West Pacific during 5–4 cal kyr BP and 4.50 (± 0.5) cal kyr BP was a transitional period, suggesting the prevalence of ENSO-like conditions over the tropical Pacific around 4.20 cal kyr BP. The stable oxygen isotopes in shells of planktonic foraminifera from the West Pacific warm pool also showed enhanced ENSO activities at about 4.20 cal kyr BP (Brijker et al., 2007).

It has been shown that weak ENSO conditions prevailed during the early and middle Holocene, while stronger than normal conditions began to emerge since (Moy et al., 2002; Tudhope et al., 2001; Haug et al., 2001; Conroy et al., 2008; Donders et al., 2008; McGregor et al., 2013). However, there is still a lack of consistency about the ENSO activity during 4.50–4.00 kyr BP. For example, many records showed

mutated ENSO activities during 5–4 cal kyr BP followed by enhanced ENSO activities after 4 cal kyr BP (Carré et al., 2014; Cobb et al., 2013; McGregor et al., 2013; Moy et al., 2002; Tudhope et al., 2001; Zhang et al., 2014). However, other records show that ENSO frequency and intensity have increased between 4.50 and 4.00 cal kyr BP (e.g., Haug et al., 2001; Conroy et al., 2008; Donders et al., 2008), and the enhanced ENSO variability culminated at ~4.10 cal kyr BP when the reef ecosystem in tropical eastern Pacific started to collapse (Fig. 3) (Toth et al., 2012; Toth et al., 2015). Model-data comparison also revealed an inconsistency of ENSO activities during the middle Holocene (Brown et al., 2008; Karamperidou et al., 2015), implying a regional difference in the expression of the ENSO and thus the complexity of the climate system (Cobb et al., 2013). This inconsistency may arise from either the ambiguous indicative meaning of the proxy records or the low temporal resolution of the sedimentary records. For example, marine sediments usually have a low depositional rate, whereas coral reefs can only document a short time period (Conroy et al., 2008). Owing to these problems, we are unable to determine whether or not ENSO was enhanced during 4.50–4.00 cal kyr BP. Nevertheless, there is a potential causal link between the 4.2-kyr event and ENSO as the global distribution of arid areas during the 4.2-kyr event resembled that of recent past when El Niño events occurred (Barron and Anderson, 2011). Strong El Niño events in the East Pacific during this period are also documented (Briker et al., 2007; Conroy et al., 2008; Toth et al., 2012). Our record indicates that the pattern of both temperature and precipitation in the Yangtze Delta resembled that of today when the ENSO occurs. Therefore, the 4.2-kyr event in this area appears to exhibit an El Niño-dominated climate.

5.5. Collapse of regional civilization linked to the ~4.2-kyr event

Our records provide clues to assess the impacts of the 4.2-ka event on the societal changes during this period. The gradual increase in the abundance of both *Altingia* and deciduous *Quercus* from ~4.50 to 4.34 cal kyr BP indicates intensifying El Niño-dominated like climate condition culminated at ~4.34 cal kyr BP (Fig. 4). The substantial increase in deciduous *Quercus* (Fig. 4) was immediately followed by a rapid decline in the abundance of *Poaceae* > 38 µm, a proxy for rice farming activities (Li et al., 2012b), suggesting that agricultural activities were absent and the Neolithic people may have emigrated from this area since 4.30 cal kyr BP. Based on published results, Liu and Chen (2012) suggested that the demise of the Liangzhu Culture occurs at about 4.00 cal kyr BP. Wang et al. (2018) synthesized published data and found that the ages of most late-Liangzhu cultural sites clustered at 4.50 cal kyr BP. Also, archaeological studies at the Mojiashan site revealed that the Liangzhu Culture began to decline at 4.50 cal kyr BP and terminated by 4.30 cal kyr BP (Wang et al., 2017). Our results indicate that the abundance of *Poaceae* > 38 µm decreased suddenly at 4.30 cal kyr BP, compatible with that of the Mojiashan site and further confirm previous conclusion about the timing of the demise of Liangzhu Culture in the Yangtze River deltaic plain. The prolonged periods of the enhanced ENSO-like climate variability was probably the culprit for the collapse of the Liangzhu cultures in East China. The impacts of the prolonged periods of ENSO-like climate variability were probably projected worldwide via atmospheric teleconnections with Asian Monsoon (e.g., Prasad et al., 2014) and the Intertropical Convergence Zone (ITCZ) (e.g., Haug et al., 2001; Conroy et al., 2008). Changes in the strength of Asian Monsoon and the latitudinal position of the ITCZ can affect the global precipitation patterns. Strong deprivation of precipitation around 4.20 cal kyr BP in many monsoonal regions such as the mid-low latitudes of Asia (Liu and Feng, 2012; Prasad et al., 2014), Africa (Ruan et al., 2016), and North America (Booth et al., 2005) has been widely documented. Prolonged droughts around 4.20 cal kyr BP associated with the prevailing ENSO-like climate variability were likely the ultimate trigger of the collapse of Neolithic civilizations in these regions (Cullen et al., 2000; Drysdale et al., 2006; Staubwasser and

Weiss, 2006; Walker et al., 2012; Liu and Feng, 2012; Dixit and Hodell, 2014).

As the 4.2-kyr event occurred at a climatic boundary condition similar to that of today and modern ENSO regime was established ~3000 to 4500 years ago (Carré et al., 2014), a similar prolonged ENSO-like condition could happen again if certain thresholds are crossed as global warming continues (Toth et al., 2015).

6. Conclusions

The well-dated, high-resolution pollen records from the Tianluoshan archaeological site in eastern China reveal that temperature and precipitation variations strikingly resemble modern ENSO variability at interdecadal time scale from ~4.50 to 4.00 cal kyr BP. Also, a shift to an overall enhanced ENSO-like variability occurred from ~4.50 to 4.30 cal kyr BP, which was immediately followed by an abrupt decline in the rice-based agriculture, suggesting that the prolonged period of ENSO dominated like climate condition may have caused the collapse of Liangzhu culture in eastern China. The impacts of prolonged periods of ENSO-like climate variability may have been projected globally via its coupling with Asia Monsoon and the ITCZ, triggering the pronounced climate anomaly 4.2 cal kyr BP.

Acknowledgments

This study was supported by the National Natural Science Foundation of China (grant nos. 41476029, 41372183, and 41401217). We thank the three anonymous reviewers for their constructive comments and suggestions. We are grateful to Editor Prof. Howard Falcon-Lang for providing insightful comments and for helping polish the language that greatly improved the manuscript.

Appendix A. Supplementary data

Supplementary data to this article can be found online at <https://doi.org/10.1016/j.palaeo.2018.07.031>.

References

- Atahan, P., Itzstein-Davey, F., Taylor, D., Dodson, J., Qin, J., Zheng, H., Brooks, A., 2008. Holocene-aged sedimentary records of environmental changes and early agriculture in the lower Yangtze, China. *Quat. Sci. Rev.* 27 (5), 556–570.
- Barron, J.A., Anderson, L., 2011. Enhanced Late Holocene ENSO/PDO expression along the margins of the eastern North Pacific. *Quat. Int.* 235, 3–12.
- Blaauw, M., Christen, J.A., 2011. Flexible paleoclimate age-depth models using an autoregressive gamma process. *Bayesian Anal.* 6, 457–474.
- Bond, G.C., Kromer, B., Beer, J., Muscheler, R., Evans, M.N., Showers, W., Hoffmann, S., Lotti-Bond, R., Hajdas, I., Bonani, G., 2001. Persistent solar influence on North Atlantic climate during the Holocene. *Science* 294, 2130–2136.
- Booth, R.K., Jackson, S.T., Forman, S.L., Kutzbach, J.E., Bettis, E.A., Kreig III, J., Wright, D.K., 2005. A severe centennial scale drought in mid-continental North America 4200 years ago and apparent global linkages. *The Holocene* 15, 321–328.
- Briker, J.M., Jung, S.J.A., Ganssen, G.M., Bickert, T., Kroon, D., 2007. ENSO related decadal scale climate variability from the Indo-Pacific Warm Pool. *Earth Planet. Sci. Lett.* 253, 67–82.
- Broecker, W.S., et al., 1989. Routing of meltwater from Laurentide Ice Sheet during the Younger Dryas cold episode. *Nature* 314, 318–321.
- Bronk Ramsey, C., 2009. Bayesian analysis of radiocarbon dates. *Radiocarbon* 51 (1), 337–360.
- Brown, J., Tudhope, A.W., Collins, M., McGregor, H.V., 2008. Mid-Holocene ENSO: issues in quantitative model-proxy data comparisons. *Paleoceanography* 23.
- Carré, M., Sachs, J.P., Purca, S., Schauer, A.J., Braconnot, P., Falcón, R.A., Julien, M., Lavallée, D., 2014. Holocene history of ENSO variance and asymmetry in the eastern tropical Pacific. *Science* 345, 1045–1048.
- Chen, S.J., 1995. Numerical simulation of El Niño and East Asia warm winter. *Acta Meteor. Sin.* 53, 380–384 (In Chinese with English abstract).
- Chen, Q.B., Wu, M.X., Tang, Z.C., 1988. *Altingia gracilipes* forest in the south of Zhejiang Province. *Journal of Zhejiang Forestry Science and Technology* 8 (3), 1–9 (in Chinese).
- Cobb, K.M., Westphal, N., Sayani, H.R., Watson, J.T., Lorenzo, E.D., Cheng, H., Edwards, R.L., Charles, C.D., 2013. Highly variable El Niño–Southern Oscillation throughout the Holocene. *Science* 339, 67–70.
- Conroy, J.L., Overpeck, J.T., Cole, J.E., Shanahan, T.M., Steinitz-Kannan, M., 2008. Holocene changes in eastern tropical Pacific climate inferred from a Galápagos lake

- sediment record. *Quat. Sci. Rev.* 27 (11–12), 1166–1180.
- Cullen, H.M., DeMenocal, P.B., Hemming, S., Hemming, G., Brown, F.H., Guilderson, T., Sirocko, F., 2000. Climate change and the collapse of the Akkadian empire: evidence from the deep sea. *Geology* 28, 379–382.
- Dixit, Y., Hodell, D.A., Petrie, C.A., 2014. Abrupt weakening of the summer monsoon in northwest India ~4100 years ago. *Geology* 42, 339–342.
- Donders, T.H., Wagner-Cremer, F., Visscher, H., 2008. Integration of proxy data and model scenarios for the mid-Holocene onset of modern ENSO variability. *Quat. Sci. Rev.* 27 (5), 571–579.
- Drysdale, R., Zanchetta, G., Hellstrom, J., Maas, R., Fallick, A., Pickett, M., Cartwright, I., Piccini, L., 2006. Late Holocene drought responsible for the collapse of Old World civilizations is recorded in an Italian cave flowstone. *Geology* 34, 101–104.
- Faegri, K., Kaland, P.E., Krzywinski, K., 1989. Textbook of pollen analysis. John Wiley & Sons Ltd.
- Gong, D.Y., Wang, S.-W., 1999. Impact of ENSO in precipitations on continents and in China. *Chin. Sci. Bull.* 44, 315–320 (in Chinese).
- Haug, G.H., Hughen, K.A., Sigman, D.M., Peterson, L.C., Rfhl, U., 2001. Southward migration of the Intertropical Convergence Zone through the Holocene. *Science* 293, 1304–1308.
- Hu, C., Henderson, G.M., Huang, J., Xie, S., Sun, Y., Johnson, K.R., 2008. Quantification of Holocene Asian monsoon rainfall from spatially separated cave records. *Earth Planet. Sci. Lett.* 266, 221–232.
- Innes, J.B., Zong, Y.Q., Chen, Z.Y., Chen, C., Wang, Z.H., Wang, H., 2009. Environmental history, palaeoecology and human activity at the early Neolithic forager/cultivator site at Kuahuqiao, Hangzhou, eastern China. *Quat. Sci. Rev.* 28 (23), 2277–2294.
- Itzstein-Davey, F., Atahan, P., Dodson, J., Taylor, D., Zheng, H.B., 2007. A sediment-based record of Lateglacial and Holocene environmental changes from Guangfulin, Yangtze delta, eastern China. *The Holocene* 17 (8), 1221–1231.
- Karamperidou, C., Di Nezio, P.N., Timmermann, A., Jin, F.F., Cobb, K.M., 2015. The response of ENSO flavors to mid-Holocene climate: Implications for proxy interpretation. *Paleoceanography* 30, 527–547.
- Kim, J.-W., Yeh, S.-W., Chang, E.-C., 2014. Combined effect of El Niño-Southern Oscillation and Pacific Decadal Oscillation on the East Asian winter monsoon. *Clim. Dyn.* 42, 957–971.
- Koutavas, A., Lynch-Stieglitz, J., Marchitto, T.M., Sachs, J.P., 2002. El Niño-like pattern in ice age tropical Pacific sea surface temperature. *Science* 297, 226–230.
- Lambeck, K., Rouby, H., Purcell, A., Sun, Y.Y., Sambridge, M., 2014. Sea level and global ice volumes from the Last Glacial Maximum to the Holocene. *Proc. Natl. Acad. Sci. U. S. A.* 111, 15296–15303.
- Li, C.Y., 1989. East China warm winter and El Niño. *Chin. Sci. Bull.* 4, 283–286 (in Chinese).
- Li, Y.X., Tornqvist, T.E., Nevitt, J.M., Kohl, B., 2012a. Synchronizing rapid sea-level rise, final LakeAgassiz drainage, and abrupt cooling 8,200 years ago. *Earth Planet. Sci. Lett.* 315–316, 41–50.
- Li, C.H., Zheng, Y.-F., Yu, S.-Y., Li, Y.-X., Shen, H.-D., 2012b. Understanding the ecological background of rice agriculture on the Ningshao Plain during the Neolithic Age: pollen evidence from a buried paddy field at the Tianluoshan cultural site. *Quat. Sci. Rev.* 35, 131–138.
- Li, C.H., Li, Y.X., Burr, G.S., 2014. Testing the accuracy of ^{14}C age data from pollen concentrates in the Yangtze Delta, China. *Radiocarbon* 56 (1), 181–187.
- Li, M.Y., Xu, Q.H., Zhang, S.R., Li, Y.C., Ding, W., Li, J.Y., 2015. Indicator pollen taxa of human-induced and natural vegetation in Northern China. *The Holocene* 25, 686–701.
- Liu, L., Chen, X., 2012. The Archaeology of China: From the Late Paleolithic to the Early Bronze Age. Cambridge University Press.
- Liu, F., Feng, Z., 2012. A dramatic climatic transition at ~4000 cal. yr BP and its cultural responses in Chinese cultural domains. *The Holocene* 22, 1181–1197.
- Liu, Y.S., Zetter, R., Ferguson, D.K., Mohr, B.A.R., 2007. Discriminating fossil evergreen and deciduous Quercus pollen: a case study from the Miocene of eastern China. *Rev. Palaeobot. Palynol.* 145, 289–303.
- Liu, Z.-Y., Wen, X.-Y., Brady, E.C., Otto-Bliessner, B., Yud, G., Lu, H.-Y., Cheng, H., Wang, Y.-J., Zheng, W.-P., Ding, W.-J., Edwards, R.L., Cheng, J., Liu, W., Yang, H., 2014. Chinese cave records and the East Asia Summer Monsoon. *Quat. Sci. Rev.* 83, 115–128.
- Liu, Y., Sun, Q.L., Fan, D.D., Lai, X.H., Xu, L.C., Finlayson, B., Chen, Z.Y., 2016. Pollen evidence to interpret the history of rice farming at the Hemudu site on the Ningshao coast, eastern China. *Quat. Int.* 426, 195–203.
- Long, S.W., Liu, J.X., Zheng, W., 2009. Study on the sowing seedling-raising of *Altingia chinensis*. *Northern Horticulture* 5, 199–201 (in Chinese).
- Long, T.W., Qin, J.G., Atahan, P., Mooney, S., Taylor, D., 2014. Rising waters: New geochronological evidence of inundation and early agriculture from former settlement sites on the southern Yangtze Delta, China. *The Holocene* 24 (5), 546–558.
- Mayewski, P.A., Rohling, E.E., Stager, J.C., Karlén, W., Maasch, K.A., Meeker, L.D., Meyerson, E.A., Gasse, F., Kreveld, S.V., Holmgren, K., Lee-Thorp, J., Rosqvist, Rack G.F., Staubwasser, M., Schneider, R.R., Steig, E.J., 2004. Holocene climate variability. *Quat. Res.* 62, 243–255.
- McGregor, H.V., Fischer, M.J., Gagan, M.K., Fink, D., Phipps, S.J., Wong, H., Woodroffe, C.D., 2013. A weak El Niño/Southern Oscillation with delayed seasonal growth around 4,300 years ago. *Nat. Geosci.* 6, 949–953.
- McPhaden, M.J., Zebiak, S.E., Glantz, M.H., 2006. ENSO as an integrating concept in earth science. *Science* 314 (5806), 1740–1745.
- Meehl, G.A., 1994. Coupled land-ocean-atmosphere processes and South Asian monsoon variability. *Science* 265, 263–267.
- Meissner, K.J., Clark, P.U., 2006. Impact of floods versus routing events on the thermohaline circulation. *Geophys. Res. Lett.* 33 (15), L15704. <https://doi.org/10.1029/2006GL026705>.
- Moy, C.M., Seltzer, G.O., Rodbell, D.T., Anderson, D.M., 2002. Variability of El Niño/Southern Oscillation activity at millennial timescales during the Holocene epoch. *Nature* 420, 162–165.
- Prasad, S., Anoop, A., Riedel, N., Sarkar, S., et al., 2014. Prolonged monsoon droughts and links to Indo-Pacific warm pool: a Holocene record from Lonar Lake, central India. *Earth Planet. Sci. Lett.* 391, 171–182.
- Reimer, P.J., Bard, E., Bayliss, A., Warren Beck, J., Blackwell, P.G., 2013. Intcal13 and Marine13 radiocarbon age calibration curves 0–50,000 years cal BP. *Radiocarbon* 55 (4), 1869–1887.
- Ruan, J., Kherbouche, F., Genty, D., Blamart, D., Cheng, H., Dewilde, F., Hachi, S., Edwards, R.L., Régnier, E., Michelot, J.-L., 2016. Evidence of a prolonged drought ca. 4200 years BP correlated with prehistoric settlement abandonment from the Guelldaman GLD1 Cave, Northern Algeria. *Clim. Past* 12, 1–14. <https://doi.org/10.5194/cp-12-1-2016>.
- Shu, J.W., Wang, W.M., Jiang, L.P., Takahara, H., 2010. Early Neolithic vegetation history, fire regime and human activity at Kuahuqiao, Lower Yangtze River, East China: new and improved insight. *Quat. Int.* 227, 10–21.
- Staubwasser, M., Weiss, H., 2006. Holocene climate and cultural evolution in late prehistoric, early historic West Asia. *Quat. Res.* 66, 72–387. <https://doi.org/10.1016/j.yqres.2006.09.001>.
- Staubwasser, M., Sirocko, F., Grootes, P., Segl, M., 2003. Climate change at the 4.2 ka BP termination of the Indus valley civilization and Holocene south Asian monsoon variability. *Geophys. Res. Lett.* 30, 1–4.
- Stott, L.K., Cannariato, K., Thunel, R.L., Haug, G.H., Koutavas, A., Lund, S., 2004. Decline in surface temperature and salinity in the western tropical Pacific ocean in the Holocene epoch. *Nature* 431, 56–59.
- Sun, D., 2000. Global climate change and El Niño: a theoretical framework. In: Diaz, H.F., Markgraf, V. (Eds.), *El Niño and Southern Oscillation*. Cambridge University Press, Cambridge, pp. 443–463.
- Toth, L.T., Aronson, R.B., Vollmer, S.V., Hobbs, J.W., Urrego, D.H., Cheng, H., Enochs, I.C., Combosch, D.J., van Woesik, R., Macintyre, I.G., 2012. ENSO drove 2500-year collapse of eastern Pacific coral reefs. *Science* 337, 81–84.
- Toth, L.T., Aronson, R.B., Cobb, K.M., Cheng, H., Edwards, R.L., Grothe, P.R., Sayani, H.R., 2015. Climatic and biotic thresholds of coral-reef shutdown. *Nat. Clim. Chang.* 5, 369–374.
- Tudhope, A.W., Chilcott, C.P., McCulloch, M.T., Cook, E.R., Chappell, J., Ellam, R.M., Lea, D.W., Lough, J.M., Shimmield, G.B., 2001. Variability in the El Niño - southern oscillation through a glacial-interglacial cycle. *Science* 291, 1511–1517.
- Walker, M.J.C., Berkelhammer, Bjork, M.S., Cwynar, L.C., Fisher, D.A., Long, A.J., Lowe, J.J., Newnham, R.M., Rasmussen, S.O., Weiss, H., 2012. Formal subdivision of the Holocene Series/Epoch, a discussion paper by a working group of the INTIMATE (Integration of ice-core, marine and terrestrial records) and the subcommission on Quaternary stratigraphy (International commission on Stratigraphy). *J. Quat. Sci.* 27, 649–659.
- Wang, X.C., 2017. Mid-Holocene Environmental Changes and Neolithic Human Activities in the Lower Yangtze Region, China: Evidence from Lacustrine Sediment. Nanjing Institute of Geography and Limnology, Chinese Academy of Sciences, Nanjing, pp. 1–109.
- Wang, P.L., Chang, K.T., 1991. The pollen morphology in relation to the taxonomy and phylogeny of Fagaceae. *Acta phytotaxonomica sinica* 29 (1), 60–66.
- Wang, F.S., Chien, N.F., Zhang, Y.L., Yang, H.Q., 1997. In: second edition (Ed.), *Pollen Flora of China*. Science Press, Beijing.
- Wang, B., Wu, R.G., Fu, X.H., 2000. Pacific-East Asian teleconnection: how does ENSO affect East Asian climate? *J. Clim.* 13, 1517–1536.
- Wang, Y.J., Cheng, H., Edwards, R.L., He, Y.-Q., Kong, X.-G., An, Z.-S., Wu, J.-Y., Kelly, M.J., Dykoski, C.A., Li, X.-D., 2005. The Holocene Asian monsoon: links to solar changes and North Atlantic climate. *Science* 308, 854–857.
- Wang, X.C., Mo, D.W., Li, C.H., Yu, S.Y., Xue, B., Liu, H., Shi, C.X., 2017. Environmental changes and human activities at a fortified site of the Liangzhu culture in eastern China: evidence from pollen and charcoal records. *Quat. Int.* 438, 189–197.
- Wang, Z.H., Ryves, D.B., Lei, S., Nian, X.M., Lv, Y., Tang, L., Wang, L., Wang, J.H., Chen, J., 2018. Middle Holocene marine flooding and human response in the south Yangtze coastal plain, East China. *Quat. Sci. Rev.* 187, 80–93.
- Weiss, H., Bradley, R.S., 2001. What drives societal collapse? *Science* 291, 609–610.
- Wu, Z.Y., 1980. *Vegetation of China*. Science Press, Beijing.
- Wu, W.X., Liu, T.S., 2004. Possible role of the “Holocene Event 3” on the collapse of Neolithic cultures around the Central Plain of China. *Quat. Int.* 117, 153–166.
- Yang, S.X., Zheng, Z., Huang, K.Y., Zong, Y.Q., Wang, J.H., Xu, Q.H., Rolett, B.V., Li, J., 2012. Modern pollen assemblages from cultivated rice fields and rice pollen morphology: application to a study of ancient land use and agriculture in the Pearl River Delta, China. *The Holocene* 22 (12), 1393–1404.
- Yi, Y., Liu, H.Y., Liu, G., Hao, Q., Wang, H.Y., 2013. Vegetation responses to mid-Holocene extreme drought events and subsequent long-term drought on the south-eastern Inner Mongolian Plateau, China. *Agric. For. Meteorol.* 178–179, 3–9.
- Yu, S.Y., Zhu, C., Song, J., Qu, W., 2000. Role of climate in the rise and fall of Neolithic cultures on the Yangtze delta. *Boreas* 29, 157–165.
- Yu, S.Y., Colman, S.M., Lowell, T.V., Milne, G.A., Fisher, T.G., Breckenridge, A., Boyd, M., Teller, J.T., 2010. Freshwater outburst from Lake Superior as a trigger for the cold event 9300 years ago. *Science* 328, 1262–1266.
- Yuan, Y., Yang, H., Li, C.-Y., 2012. Influence on the subsequent summer precipitation in China by different types of El Niño events. *Acta Meteor. Sin.* 70, 467–478 (in Chinese with English abstract).
- Zhang, Q., Zhu, C., Liu, C.L., Jiang, T., 2004. Environmental changes in the Yangtze Delta since 7000 a BP. *Acta Geograph. Sin.* 59 (4), 534–542 (In Chinese with English abstract).
- Zhang, Z.H., Leduc, G., Sachs, J.P., 2014. El Niño evolution during the Holocene revealed

- by a biomarker rain gauge in the Galapagos Islands. *Earth Planet. Sci. Lett.* 404, 420–434.
- Zhao, Z.G., 1989. El Niño and temperature variation in China. *Meteor-Forschung* 15, 26–30 (in Chinese with English abstract).
- Zhejiang Provincial Institute of Cultural Relics and Archaeology, 2014. *Bianjiashan*. Cultural Relics Press, Beijing.
- Zheng, Z., Huang, K.Y., Xu, Q.H., Lu, H.Y., Cheddadi, R., Luo, Y.L., Beaudouin, C., Luo, C.X., Zheng, Y.W., Li, C.H., Wei, J.H., Du, C.B., 2008. Comparison of climatic threshold of geographical distribution between dominant plants and surface pollen in China. *Sci. China Ser. D Earth Sci.* 51 (8), 1107–1120.
- Zheng, Z., Wei, J.H., Huang, K.Y., Xu, Q.H., Lu, H.Y., Tarasov, P., Luo, C.X., Beaudouin, C., Deng, Y., Pan, A.D., Zheng, Y.W., Luo, Y.L., Nakagawa, T., Li, C.H., Yang, S.X., Peng, H.H., Cheddadi, R., 2014. East Asian pollen database: modern pollen distribution and its quantitative relationship with vegetation and climate. *J. Biogeogr.* 41, 1819–1832.
- Zhu, C., Song, J., You, K.Y., 1996. Formation of the culture interruption of the Maqiao site, Shanghai. *Chin. Sci. Bull.* 41 (2), 148–152 (in Chinese).
- Zong, Y., Wang, Z.H., Innes, J.B., Chen, Z., 2012. Holocene environmental change and Neolithic rice agriculture in the lower Yangtze region of China: a review. *The Holocene* 22 (6), 623–635.